Theoretical model of shear capacity of steel fiber reinforced concrete beams

Lantsoght, Eva O.L.

DOI
10.1016/j.engstruct.2023.115722

Publication date
2023

Document Version
Final published version

Published in
Engineering Structures

Engineering Structures 280 (2023) 115722

Contents lists available at ScienceDirect

Engineering Structures

journal homepage: www.elsevier.com/locate/engstruct

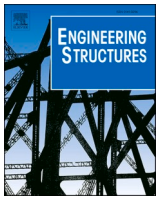

Theoretical model of shear capacity of steel fiber reinforced concrete beams

Eva O.L. Lantsoght [a,b,*]

[a] Politécnico, Universidad San Francisco de Quito USFQ, Diego de Robles y Pampite, Sector Cumbaya, EC 170157 Quito, Ecuador
[b] Concrete Structures, Department of Engineering Structures, Delft University of Technology, Stevinweg 1, 2628CN Delft, The Netherlands

ARTICLE INFO

Keywords:
Aggregate interlock
Cracking
Dowel action
Fiber properties
Fiber type
Mechanical properties
Steel fibers
Shear

ABSTRACT

One of the barriers to implementation of steel fiber reinforced concrete (SFRC) into structural applications is the lack of understanding of the shear behaviour of SFRC members. This paper proposes a theoretical model for the shear capacity of SFRC members with mild steel reinforcement based on the shear-carrying mechanisms and sectional analysis. The model is derived completely theoretically, based on concepts from the literature, and does not include new empirical aspects. The approach is then compared to 323 experiments from the literature of beams with slender, rectangular cross-sections failing in shear. It is found that the model is slightly conservative, and experimental research necessary to further develop the model is described. The presented theory aims to be a framework for a fully theoretical description of the shear capacity of SFRC members with longitudinal reinforcement and without shear reinforcement.

1. Introduction

Mixes of concrete that contain dispersed fibers were proposed as early as 1874 (in a patent by A. Bernard) [1]. Even though the idea is not new, structural applications of steel fiber reinforced concrete (SFRC) are currently limited to joints with a closing function, small housing projects, industrial buildings, and tunnels [2]. The reason why the construction industry is slow to adopt the material is that not all building and bridge codes contain a full set of design equations for members with SFRC. ACI 318-9 [3], for example, mentions in terms of shear capacity of SFRC only that 0.75 % of fibers can be used to replace minimum shear reinforcement, but the code does not include equations to verify the shear capacity of reinforced or prestressed concrete members that contain (steel) fibers. Design equations for SFRC members are not present in all building and bridge codes because mechanical models that can serve as a theoretical basis for code equations are lacking. In particular, a solid theoretical understanding of the shear capacity of SFRC members with longitudinal reinforcement and without transverse reinforcement is missing [4].

There are various benefits associated with adding fibers to concrete. The fibers add tensile strength to the mixture and improve the post-cracking behavior [5], reduce the post-peak rate of strength loss in compression tests [6], result in smaller and better distributed cracks in concrete members [7], increase the flexural capacity [8], improve the fatigue life for cases without stress reversals [9,10], and reduce the effects of creep in normal strength SFRC beams with stirrups under sustained loading [11].

This paper studies the shear capacity of SFRC members with longitudinal reinforcement and without stirrups from a theoretical perspective. The scope of this work is normal strength SFRC members. It is only briefly explored if tension-stiffening ultra-high performance fiber reinforced concrete (UHPFRC) [12,13] can be addressed with the same model. The shear capacity is derived by summing the contributions of aggregate interlock [14], dowel action [15], capacity in the tension zone [16], and capacity of the uncracked concrete in the compression zone [17], considering the mechanical properties of SFRC [4], the sectional equilibrium of SFRC [18,19], and the effect of fibers on crack width and spacing [20]. As such, it is an extension of the Critical Shear Displacement Theory to include the effect of steel fibers [21,22]. Fig. 1 shows the different shear-carrying mechanisms that play a role in SFRC. No new empirical aspects are introduced into this theoretical model. As such, the proposed model can serve as a basis for future experimental work to improve the model, as well as a solid basis rooted in the mechanics of the problem for code equations for the shear capacity of SFRC.

2. Literature review

The majority of expressions that have been proposed to estimate the shear capacity of SFRC members with longitudinal steel reinforcement are empirical in nature [4]. The existing code equations for the shear capacity of SFRC from France [23] (which is geared towards UHPFRC),

* Corresponding author.
E-mail address: elantsoght@usfq.edu.ec.

https://doi.org/10.1016/j.engstruct.2023.115722
Received 21 April 2022; Received in revised form 12 December 2022; Accepted 26 January 2023
Available online 3 February 2023

Nomenclature

Notation List

a	shear span; center-to-center distance between load and support
a_{exp}	factor in trendline between V_{test}/V_{pred} and parameter under consideration: $y = a_{exp}x + b_{exp}$ with $y = V_{test}/V_{pred}$ and x the studied parameter
a_v	clear shear span; face-to-face distance between load and support
b	width of rectangular cross-section
b_n	nominal web width of cross-section
c	height of concrete compression zone
c_a	the effective concrete cover
d	effective depth of cross-section
$d_{a,\max}$	maximum aggregate size
d_f	fiber diameter
f_c	concrete compressive strength
f_{c1}	concrete compressive stress in elastic stage
f_{c2}	concrete compressive stress in plastic branch of stress-strain diagram,
f_{t1}	concrete tensile stress in elastic stage
f_{t2}	concrete tensile stress in post-cracking stage
f_{tenf}	tensile strength of steel fibers
f_s	stress in the steel
f_{sy}	yield stress of the steel
h	height of rectangular cross-section
h_{c1}	height of compression zone in elastic stage
h_{c2}	height of compression zone in plastic branch of stress-strain diagram
h_{t1}	height of tension zone in elastic stage
h_{t2}	height of tension zone in post-cracking stage
k	neutral axis depth ratio
k_i	neutral axis depth ratio for stage i, with $i = 1$, 21, 22, 31, or 32
k_f	factor accounting for the fiber effectiveness due to the fiber aspect ratio
l	span length
l_f	length of fiber
n	modular ratio (E_s/E)
n_i	parameters used in calculating the crack spacing
n_s	number of reinforcement bars on one line in the cross-section
s_b	a parameter representative of the effective longitudinal bar spacing
s_{cr}	crack spacing
s_m	average stabilized crack spacing
s_{mi}	the reinforcement effectiveness parameter
w_b	crack width at the bottom of the crack
$w_{cr,avg}$	average crack width
$w_{cr,\max}$	maximum crack width
y_{c1}	internal lever arm from neutral axis to resultant of concrete in compression in elastic range
y_{c2}	internal lever arm from neutral axis to resultant of concrete in compression in plastic branch of stress-strain diagram
y_s	internal lever arm from neutral axis to tension steel
y_{t1}	internal lever arm from neutral axis to resultant of concrete in tension in elastic stage
y_{t2}	internal lever arm from neutral axis to resultant of concrete in tension in post-cracking stage
z	internal lever arm from centroid of tension to centroid of compression
A_s	area of reinforcement steel
B_i	coefficient, with $i = 1.0.5$
C_c	resultant of concrete under compression
C_i	coefficient, with $i = 1.0.11$
E	Young's modulus of SFRC in tension
E_c	Young's modulus of SFRC in compression
E_s	Young's modulus of reinforcement steel
F	fiber factor
F_{c1}	resultant of concrete in compression in elastic stage
F_{c2}	resultant of concrete in compression in plastic branch of the stress-strain diagram
F_s	resultant force of steel in tension
F_{t1}	resultant of concrete in tension in elastic stage
F_{t2}	resultant of concrete in tension in post-cracking stage
M'	normalized bending moment
M'_i	normalized bending moment for stage i, with $i = 1$, 21, 22, 31, or 32
M_{cr}	cracking moment of the cross-section
M_{ult}	ultimate flexural capacity
R_{sup}	support reaction force
R^2	coefficient of determination to indicate goodness of fit
T_s	resultant of steel under tension
V	sectional shear
V_a	shear resistance provided by aggregate interlock
V_{ax}	projection on the x-direction of the aggregate interlock resultant
V_{ay}	projection on the x-direction of the aggregate interlock resultant
V_{calc}	calculated shear resistance
V_{cz}	shear resistance provided by the concrete compression zone
V_d	shear resistance provided by the dowel action
V_f	volumetric fiber content
V_{flex}	sectional shear associated with the flexural capacity
$V_{fl,s}$	flexural shear capacity as determined with proposed model
V_F	shear resistance provided by the fibers in the tension zone
V_{test}	tested shear capacity
α	normalized depth of steel reinforcement (d/h)
α_f	fiber orientation factor
β	normalized tensile strain ($\varepsilon_t/\varepsilon_{cr}$)
β_{tu}	normalized tensile strain at the ultimate in tension ($\varepsilon_{tu}/\varepsilon_{cr}$)
γ	normalized concrete compressive modulus (E_c/E)
ε	used generally as strain in concrete when presenting the stress-strain diagram
ε_1	strain at maximum tensile stress of SFRC
ε_2	strain at σ_2
ε_3	25‰, end of stress-strain diagram for SFRC as proposed by RILEM [28]
ε_c	strain in the concrete in compression
$\varepsilon_{c,top}$	strain in the layer of concrete that is most in compression
ε_{cr}	strain at which SFRC cracks
ε_{cy}	strain of SFRC at yielding in compression
ε_{cu}	crushing strain of concrete
ε_s	strain in the reinforcement steel
ε_{sy}	yield strain of reinforcement steel
ε_t	strain in SFRC in tension
$\varepsilon_{t,avg}$	average tensile strain
$\varepsilon_{t,bot}$	strain in the section in the layer of concrete that is most in tension
$\varepsilon_{t,\max}$	largest tensile strain in cross-section
$\varepsilon_{t,\min}$	smallest tensile strain in cross-section
ε_{tu}	ultimate strain of SFRC in tension
ϕ_b	bar diameter
κ	normalized yield strain of the steel ($\varepsilon_{sy}/\varepsilon_{cr}$)
λ	normalized compressive strain ($\varepsilon_c/\varepsilon_{cr}$)
λ_{cu}	normalized compressive strain at the ultimate in compression ($\varepsilon_{cu}/\varepsilon_{cr}$)
λ_{R1}	normalized compressive strain at the end of elastic region 1

μ	normalized residual tensile strength (σ_p/σ_{cr})	σ_c	stress in the SFRC in compression
ρ	steel reinforcement ratio to the effective concrete cross-section area	σ_{cr}	stress at which SFRC cracks
ρ_f	fiber bond factor: 1 for hooked fibers, 0.75 for crimped fibers, 0.5 for straight fibers	σ_{cy}	stress at yielding of the concrete in compression
ρ_g	steel reinforcement ratio to the gross concrete cross-section area	$\sigma_{f,cr}$	distributed shear resistance as provided by the steel fibers crossing the shear crack in the tension zone
$\rho_{s,eff}$	the effective reinforcement ratio	σ_p	constant stress after cracking in SFRC in tension
σ	stress in the concrete when presenting the stress-strain diagram	σ_t	stress in the SFRC in tension
σ_1	maximum tensile stress in SFRC	τ	fiber-concrete bond stress
σ_2	post-peak tensile stress in SFRC	φ_b	diameter of reinforcement bar
σ_3	tensile stress in SFRC for a strain of 25‰	ω	normalized concrete compressive yield strain ($\varepsilon_{cy}/\varepsilon_{cr}$)
		Δ	shear displacement
		Δ_{cr}	critical shear displacement

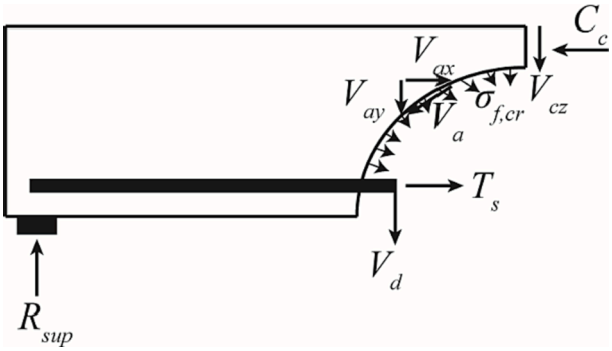

Fig. 1. Shear-carrying mechanisms in SFRC, reprinted from [4].

the German guideline for SFRC [24], and the equations as proposed by the *fib* Model Code 2010 [25] (which are based on the Modified Compression Field Theory [26] and the use of various Levels of Approximation [27]) and by RILEM [28] are empirical in nature.

Only a handful of mechanical models for SFRC exist, none of which address the contributions of all four shear-carrying mechanisms (tensile capacity in the tension zone, compression capacity in the uncracked zone, aggregate interlock, and dowel action). The dual potential capacity model [29,30], for example, derives the shear capacity based on the tensile capacity of the fiber concrete in the tension zone and the compressive capacity of the concrete in the uncracked compression zone. The Multi-Action Shear Model (MASM) [31] considers the compression capacity in the uncracked zone, dowel action, and lumps together the effect of the shear-mechanisms that act on the shear crack (aggregate interlock and tensile capacity in the tension zone) into a contribution that is mostly governed by the steel fibers. The MASM assumes that failure occurs when the combination of normal and shear stresses in the compression chord reach Kupfer's [32] biaxial failure envelope.

Models based on the theory of plasticity are also derived for SFRC. The first available model in the literature follows from modifying the lower-bound plasticity-based model for a reinforced concrete member subjected to shear [33]. This approach resulted in a practical method to determine the shear capacity of a SFRC member [34]. As expected from a lower-bound plasticity-based model, this approach resulted in conservative predictions when compared to experimental data. Another model [35,36], based on the upper-bound theory of plasticity for members in shear [37,38] and the connection to the bending moment capacity, was proposed in the past as well. Most work on plasticity-based models for SFRC was done in the 1980s and 1990s. A recent model [39–41] considers concepts of the theory of plasticity using the crack sliding model for shear [42,43] in reinforced concrete, combined with the arching action in deep beams [44], the post-cracking tensile strength of the SFRC and the resulting ability to control sliding along the shear cracks. This model also studied the influence of steel fibers on the size effect [45].

A family of models for the shear capacity of SFRC results from extending the Modified Compression Field Theory (MCFT) to include the effect of the steel fibers. The MCFT uses smeared cracking and a constitutive model for cracked concrete, and the extensions of the MCFT for SFRC use similar assumptions. For example, the proposal by Zhang [46] is based on an alteration of the constitutive model for cracked concrete, so that it includes the effect of the fibers, with cracked SFRC as a new material with its own constitutive model. In particular, this constitutive model considers the contribution of the fibers to transfer of stresses across the main crack at and after the peak.

Another approach based on the MCFT is the Disturbed Stress Field Model [47,48], which is a more general approach that requires the use of finite element software for implementation. A simplification of this approach is a model [49] that relates the average tensile stress to the tensile stress in a steel fiber at a crack. This information then results in the strain profiles in the SFRC member, consisting of the net strain and slip. This approach can also be programmed into finite element software and has been worked into VecTor 2 [50].

Since the constitutive models for cracked concrete used in the MCFT are compared to panel tests, a similar approach was also followed for SFRC [51,52], resulting in proposed constitutive models for the cracked SFRC [53]. These constitutive models include the large softening of the SFRC under tension, as also observed in the panel tests. As such, this approach would not be valid for tension-hardening concrete materials with fibers, such as UHPFRC.

Another MCFT-based model at the meso-level studied the rotation of the fibers individually [54], which resulted in simplified expressions that can be used for design [55]. Additionally, a simplified design expression based on the MCFT was proposed [56] for inclusion in the *fib* Model Code 2010 [25], so that the proposed approach is in line with all shear expressions in the *fib* Model Code. The latter approach is the most pragmatic set of expressions based on the MCFT and is aimed at practicing engineers.

Another mechanical model for the shear capacity of SFRC is a more general approach [57] based on the softened truss model of Hsu [58,59], which resulted in a softened truss model with steel fibers (STM-SF).

3. Theoretical model

3.1. Sectional equilibrium

The shear-carrying mechanisms V_{cz}, the contribution of the concrete compression zone to the shear capacity, and V_F, the contribution of the fibers in the tension zone to the shear capacity, are related to the parts of the cross-section that are in compression and tension. As such, it is necessary to write out the sectional equilibrium of the SFRC and determine the height of the compression zone and the height of the

tension zone. Fig. 2 shows the principles of sectional analysis as applied to SFRC, using the stress–strain diagram proposed by RILEM [28] and sketched in Fig. 3.

Mobasher et al. [18] proposed an analytical solution for the sectional analysis of SFRC, based on simplified material models. Fig. 4 shows the simplified material models on which the analytical solutions of the cross-section are based. Fig. 5 then shows the strains and stresses for the sectional analysis using these material models, divided into three stages: (1) stage 1, for which the stress–strain behavior is elastic in tension and compression; (2) stage 2, for which the concrete is elastic in compression and the post-cracking behavior in tension is considered; and (3) stage 3, for which the concrete is plastic in compression and the post-cracking behavior in tension is considered. For each of these three stages, the normalized neutral axis k and normalized bending moment M' can be determined as given in Table 1. The height of the compression zone can be found as kh and the bending moment is:

$$M_i = M_i' M_{cr} \tag{1}$$

with the cracking moment M_{cr}:

$$M_{cr} = \frac{1}{6} b h^2 E \varepsilon_{cr} \tag{2}$$

The steel reinforcement ratio is expressed relative to the gross cross-section area as:

$$\rho_g = \frac{A_s}{bh} \tag{3}$$

The coefficients in Table 1 are:

$$B_1 = \lambda^2 + 2\mu(\lambda+1) - 1; B_2 = \mu - 9\rho_g\lambda; B_3 = 9\rho_g\left(\rho_g 9\lambda^2 - 2\mu\lambda\right) + \mu^2; B_4 = 2\lambda\left(9\rho_g\kappa + \mu\right) B_5 = 20\lambda - 101 + 2\mu(\lambda+1)$$

$$C_1 = 0; C_2 = 27\rho_g + 3; C_3 = -3 - 54\rho_g\alpha; C_4 = 1 + 27\rho_g\alpha^2; C_5 = 2\lambda^3 + 3\mu\left(\lambda^2 - 1\right) + 2; C_6 = 6\lambda^2\left(9\lambda\rho_g - \mu\right) C_7 = 3\lambda^2\left(\mu - 36\rho_g\alpha\lambda\right); C_8 = 54\rho_g\alpha^2\lambda^3; C_9 = -6\lambda^2\left(9\rho_g\kappa + \mu\right); C_{10} = 3\lambda^2\left(18\rho_g\alpha\kappa + \mu\right) C_{11} = 30\lambda^2 + 3\mu\left(\lambda^2 - 1\right) - 998$$

3.2. Contribution of concrete compression zone

The contribution of the concrete in the compression zone to the shear capacity can be expressed based on the classical equation as proposed by Mörsch [60]:

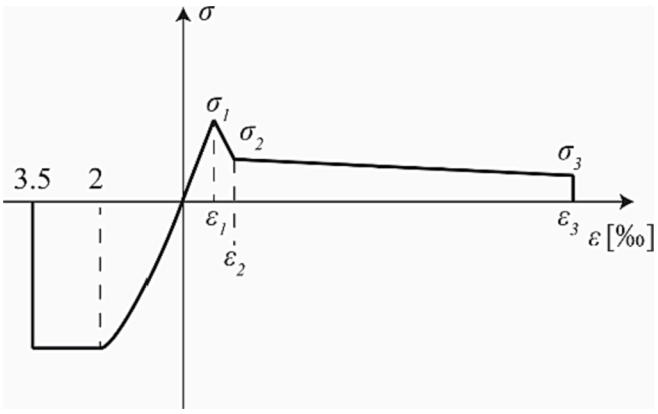

Fig. 3. Stress–strain relationship for fiber concrete, based on the RILEM recommendations [28].

$$V_{cz} = \frac{2}{3}\frac{kh}{z} V \tag{4}$$

The expression is the same as for regular reinforced concrete, and the values of kh and z can be adjusted to reflect the equilibrium in the SFRC cross-section. Since the total sectional shear capacity V needs to be known, the value of V_{cz} is determined iteratively.

3.3. Dowel action

The contribution of dowel action to the shear capacity can be expressed with the classical expression of Baumann and Rüsch [61]:

$$V_d = 1.64 b_n \phi_b f_c^{1/3} \tag{5}$$

with f_c the concrete compressive strength in MPa. The nominal width is determined as:

$$b_n = b - n_s \phi_b \tag{6}$$

3.4. Aggregate interlock

The contribution of aggregate interlock to the shear capacity is determined with the expression proposed by Yang [21,22,62], which is based on the fundamental analysis of aggregate interlock by Walraven [14,63]:

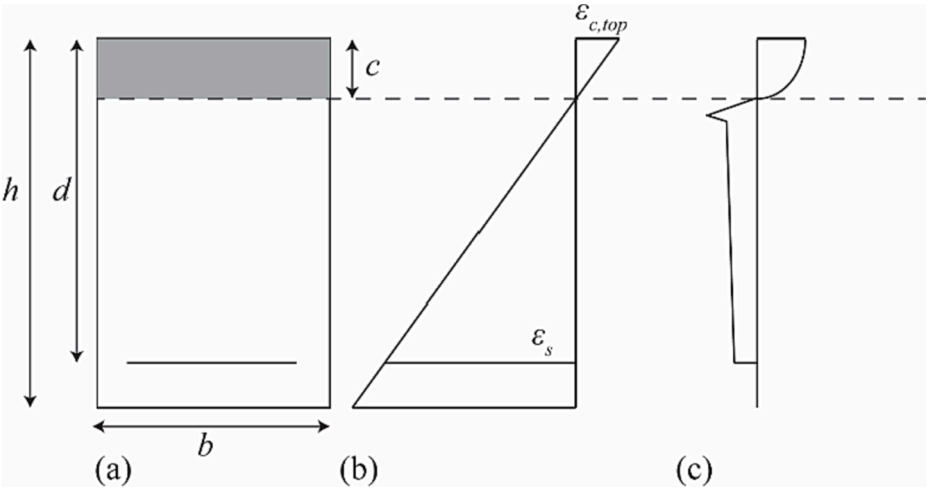

Fig. 2. Sectional analysis principles for SFRC: (a) cross-section, (b): strains (using linear strain assumption); (c) stresses: using parabolic stress–strain assumption for concrete under compression and softening behavior for SFRC in tension.

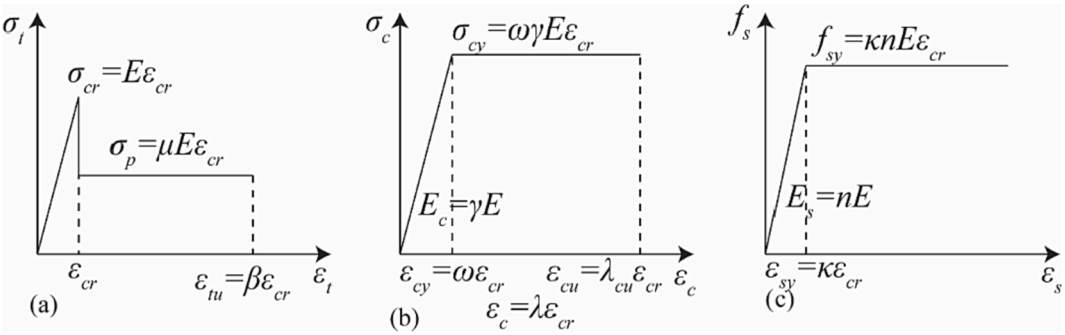

Fig. 4. Simplified material models and dimensionless constants: (a) SFRC in tension; (b) SFRC in compression; (c) reinforcement steel. Based on [18].

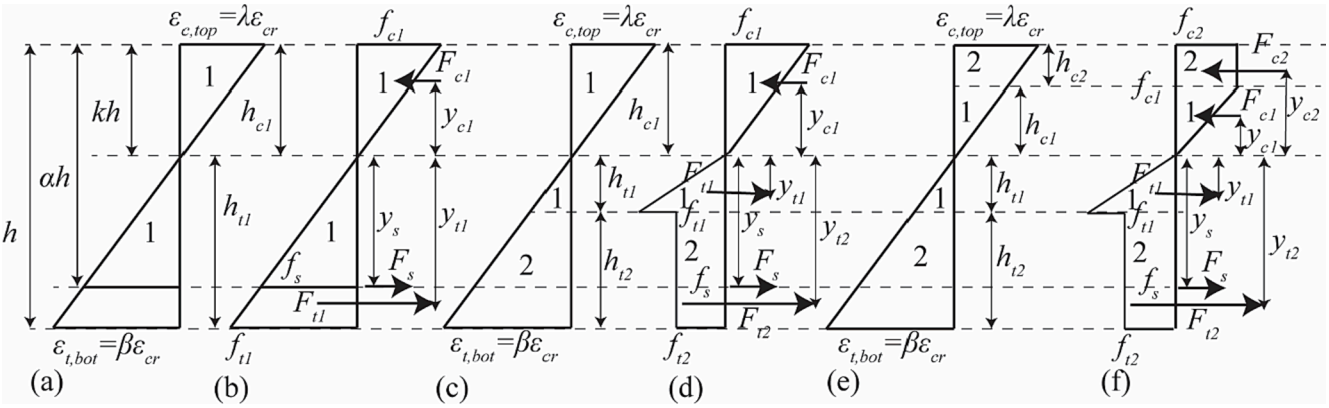

Fig. 5. Sectional analysis at three stages as a function of λ: (a) strain and (b) stress and resultant forces at stage 1 ($0 < \lambda \leq \lambda_{R1}$) of elastic compression and elastic tension; (c) strain and (d) stress and resultant forces at stage 2 ($\lambda_{R1} < \lambda \leq \omega$) of elastic compression and post-crack tension; (e) strain and (f) stress and resultant forces at stage 3 ($\omega < \lambda \leq \lambda_{cu}$) of plastic compression and post-crack tension. Based on [18].

Table 1
Normalized neutral axis k, and normalized bending moment for each stage of the normalized compressive strain at the top fiber λ. Based on [18].

Stage	steel strain	k	M′
1		$k_1 = \frac{18\rho_g\alpha - 1}{18\rho_g + 2}$	$M_1' = \frac{2\lambda}{k_1}(C_1k_1^3 + C_2k_1^2 + C_3k_1 + C_4)$
2.1	$\varepsilon_s \leqslant \varepsilon_y$	$k_{21} = \frac{\lambda}{B_1}(B_2 + \sqrt{B_3 + 2\alpha\rho_g nB_1})$	$M_{21}' = \frac{1}{\lambda^2 k_{21}}(C_5k_{21}^3 + C_6k_{21}^2 + C_7k_{21} + C_8)$
2.2	$\varepsilon_s > \varepsilon_y$	$k_{22} = \frac{B_4}{B_1}$	$M_{22}' = \frac{l}{\lambda^2}(C_5k_{22}^2 + C_9k_{22} + C_{10})$
3.1	$\varepsilon_s \leqslant \varepsilon_y$	$k_{31} = \frac{\lambda}{B_5}(B_2 + \sqrt{B_3 + 2\alpha\rho_g nB_5})$	$M_{31}' = \frac{1}{\lambda^2 k_{31}}(C_{11}k_{31}^3 + C_6k_{31}^2 + C_7k_{31} + C_8)$
3.2	$\varepsilon_s > \varepsilon_y$	$k_{32} = \frac{B_4}{B_5}$	$M_{32}' = \frac{1}{\lambda^2}(C_{11}k_{32}^2 + C_9k_{32} + C_{10})$

$$V_a = f_c^{0.56} s_{cr} b \frac{0.03}{w_b - 0.01}\left(-978\Delta^2 + 85\Delta - 0.27\right) \quad (7)$$

with $w_b \geq 0.04$ mm and f_c limited to 60 MPa. In the Critical Shear Displacement Theory, the trigger for failure is set at a certain value of the critical shear displacement (i.e. slipping of the crack) at the level of the longitudinal reinforcement. This failure criterion is different from the traditionally-used failure triggered by the unstable propagation of the shear crack. The critical shear displacement is given as:

$$\Delta_{cr} = \frac{25d}{30610\phi_b} + 0.0022 \leqslant 0.025 \text{ in mm units}$$

To calculate w_b for a SFRC member, the crack model from [20] is applied. The maximum crack width is determined as:

$$w_{cr,\max} = \left(1.7 + 3.4\frac{V_f l_f}{d_f}\right) w_{cr,avg} \quad (9)$$

The average crack width, $w_{cr,avg}$ can be determined as the product of the stabilized crack spacing s_m and the average tensile strain in the member $\varepsilon_{t,avg}$:

$$w_{cr,avg} = s_m \varepsilon_{t,avg} \quad (10)$$

In the members evaluated in this study, the strain distribution is assumed as shown in Fig. 5. As a result, the average tensile strain is:

$$\varepsilon_{t,avg} = \frac{h - kh}{2kh}\lambda\varepsilon_{cr} \quad (11)$$

The stabilized crack spacing is proposed [20] as:

$$s_m = 2\left(c_a + \frac{s_b}{10}\right)n_3 + \frac{n_1 n_2}{s_{mi}} \quad (12)$$

The effective concrete cover c_a is estimated as 1.5 times the maximum aggregate size. The parameter that represents the effective longitudinal bar spacing is:

$$s_b = 0.5\sqrt{\frac{\pi\phi_b^2}{\rho_{s,eff}}} \leqslant 15\phi_b \quad (13)$$

The reinforcement effectiveness factor is determined as:

$$s_{mi} = \frac{\rho_{s,eff}}{\phi_b} + k_f \frac{\alpha_f V_f}{d_f} \tag{14}$$

The fiber orientation factor α_f can be taken as 0.5 for the random 3-D orientation of fiber in infinitely large elements. The fiber effectiveness factor due to the fiber aspect ratio k_f is determined as:

$$k_f = \frac{l_f}{50 d_f} \geqslant 1.0 \tag{15}$$

The factors n_1, n_2, and n_3 are determined as follows: n_1 accounts for the bond properties of the main longitudinal reinforcement, with $n_1 = 0.4$ for ribbed bars and $n_1 = 0.8$ for plain bars and tendons. The factor n_2 is a function of the strain distribution across the cross-section, and is generally given as:

$$n_2 = \frac{0.25\left(\varepsilon_{t,\max} + \varepsilon_{t,\min}\right)}{2\varepsilon_{t,\max}} \tag{16}$$

For the linear strain distribution from Fig. 5, Eq. becomes $n_2 = 0.125$. For a uniaxial strain condition, $n_2 = 0.25$. Finally, n_3 is a factor related to the fiber content, determined as:

$$n_3 = 1 - \frac{\min\left(V_f, 0.015\right)}{0.015}\left(1 - \frac{1}{k_f}\right) \tag{17}$$

To determine the aggregate interlock contribution for SFRC, s_{cr} from Eq. (7) can be replaced by s_m from Eq. (13) and w_b from Eq. (7) can be replaced by $w_{cr,\max}$ from Eq. (9).

3.5. Fibers in tension zone

The contribution of the fibers in the tension zone of the cross-section is determined with the formula proposed by Mansur et al. [64]:

$$V_F = 0.41 \tau F b d \tag{18}$$

with τ in MPa, given as:

$$\tau = 0.68\sqrt{f_c} \tag{19}$$

with f_c in MPa. The fiber factor F is a measure of the fiber–matrix interfacial bond, and is a function of various properties of the fiber:

$$F = \frac{l_f}{d_f} V_f \rho_f \tag{20}$$

The fiber bond factor ρ_f is a function of the type of fiber, and equals 1 for hooked fibers, 0.75 for crimped fibers, and 0.5 for straight fibers.

In the original expression of Mansur et al. [64], the action of the fibers is assumed to work over the entire effective depth d. In the proposed model, the action of the fibers works only over the tension zone $d - kh$. Moreover, when the contribution of the fibers is large, the assumed mechanical behaviour is not correct anymore. In other words, for large amounts of fibers, the equilibrium of the contribution of the concrete in the compression zone, dowel action, aggregate interlock, and capacity of fibers in the tension zone does not hold true. Instead, the section starts to behave as a shear-reinforced section, and a different equilibrium state, often visualized as a truss with compression strut and tension ties, develops. Therefore, in this model, the contribution of the fibers is limited to a maximum value of $F = 1$. With these two alterations, Eq. (18) becomes:

$$V_F = 0.41 \times 0.68\sqrt{f_c} \times \min(1, F) \times b \times (d - kh) \tag{21}$$

3.6. Resulting theoretical model

The flexural shear capacity as determined with the proposed model can be calculated as:

$$V_{fl,s} = V_{cz} + V_d + V_a + V_F \tag{22}$$

Since this model determines a flexural shear capacity, the influence of arching action is not considered. Shear-compression [65] capacities tend to be higher than the flexural shear capacities, as a compression arch can develop between the point of application of the load and the support. Moreover, in prestressed members, web shear cracking (also called shear-tension cracking) can develop, which is based on different mechanics and not covered by the presented model [66].

In addition, it is also necessary to check if the flexure shear capacity does not exceed the theoretically determined flexural capacity of the cross-section. The flexural capacity of the cross-section is M_{ult}, which can be determined with Table 1 and Eq. (1). To compare the flexural capacity to the shear capacity, the sectional shear associated with the flexural capacity is determined as:

$$V_{flex} = \frac{M_{ult}}{a} \tag{23}$$

This expression is valid for a simply supported beam subjected to a single concentrated load. For other loading and support configurations, the value of V_{flex} can be derived from statics.

Bringing everything together, the flowchart of Fig. 6 shows how all previously described aspects of the theoretical model work together in finding the solution for the flexural shear capacity. The key element here is the sectional equilibrium, as explained in section 3.1. Ultimately, the application is illustrated in Fig. 7 to show how the different values of the shear-carrying contributions are calculated as a function of the height of the concrete compression zone, and how the solution results from equating internal shear resistance to externally applied shear. Note that the flowchart shows the way in which the solution is programmed, using the full moment–curvature diagram of the section. The point on this diagram at which a shear failure is reached is sought and the value of the neutral axis is found so that all contributions can be calculated. The proposed model follows the strain compatibility from [18] at all steps.

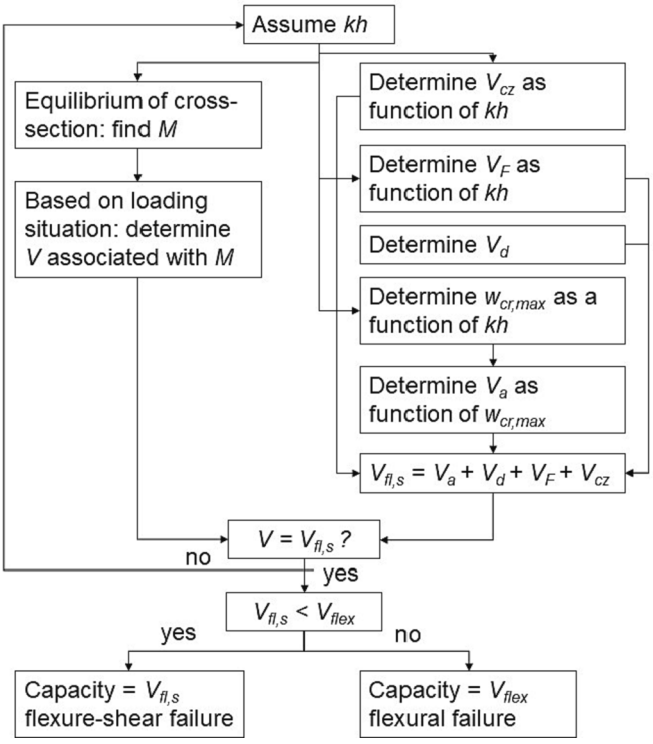

Fig. 6. Flowchart of solution strategy with proposed model. Note that this solution strategy shows the programming routines followed, and that strain compatibility is maintained.

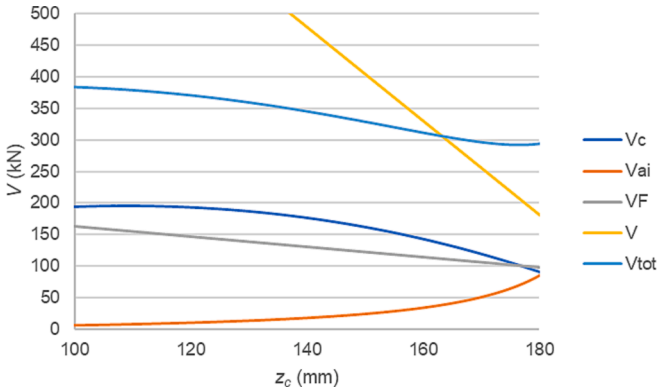

Fig. 7. Illustration of contributions as function of height of compression zone, for experiment U-0-f-3.5 by [67].

4. Database of experiments

To compare the proposed theoretical model to experiments, a subset from a larger database of shear tests [68] on SFRC with longitudinal reinforcement was extracted. The original database had 488 experiments. To derive the subset, the experiments with $a < 2.5d$, the non-rectangular cross-sections, and the lightweight specimens were removed. The resulting subset contains 323 experiments from various literature Refs. [36,40,57,64,67,69–106].

The ranges of parameters of the specimens in the subset are given in Table 2. All specimens have rectangular cross-sections. While the majority of the specimens are relatively small in scale, a number of larger specimens are also included in the database. To exclude shear-compression failures, no experiments with $a/d < 2.5$ are included in the database. The reinforcement ratio ρ shows that a few members with low reinforcement ratios as well as members with extremely high reinforcement ratios feature in the database. The yield strength of the steel and of the steel fibers covers regular reinforcement types, and some experiments with very high strength steel fibers are present in the database as well. The concrete mixes in the database include both regular SFRC as well as some experiments with UHPFRC, to see if the model can be extended to strain-hardening materials. This range is also reflected by the maximum aggregate sizes present in the database, with the smaller maximum aggregate sizes as used in UHPFRC mixes. The fiber volume fraction ranges between low amounts of fibers (0.22 %) and amounts of fibers that may become difficult to work with in the laboratory and in the field (3 %).

5. Comparison between theoretical prediction and capacity of database experiments

5.1. Results of comparison

Fig. 8 shows the comparison between the shear capacity as calculated with the proposed model (Fig. 6), V_{calc}, and the sectional shear at failure V_{test}, as caused by the self-weight of the specimen and the externally applied load(s), for the 323 experiments. The capacity of 13 experiments is determined by the flexural capacity. The average value of the tested to predicted ratio is 1.50, with a standard deviation of 0.399 and a coefficient of variation of 26.6 %. The minimum value of the tested to predicted ratio is 0.759 and the maximum value is 3.228. The 5 % lower bound as taken from the distribution of tested to predicted results is 0.932. Fig. 8a indicates that the shear capacity tends to be underestimated more as this capacity increases. In other words, the tendency for the results is to move away from the bisector line as the values increase. Fig. 8b illustrates the histogram of the results, indicating that the distribution resembles a lognormal distribution.

Table 2
Ranges of parameters in subset of database (323 experiments), as well as parameters of comparison to model.

Parameter	Min	Max	a_{exp}	R^2
l (mm)	510	7823.2	3×10^{-5}	0.0137
b (mm)	63.5	610	0.0012	0.0415
a/d (-)	2.5	6	−0.0695	0.0132
d (mm)	85.25	1118	0.0005	0.0536
ρ (%)	0.37	5.72	0.1096	0.0618
f_{sy} (MPa)	276	610	0.0002	0.0016
f_c (MPa)	9.77	215	0.0002	9×10^{-5}
$d_{a,max}$ (mm)	2	22	0.0064	0.0068
V_f (%)	0.22	3	0.0946	0.0118
f_{tenf} (MPa)	260	4913	0.0002	0.0328

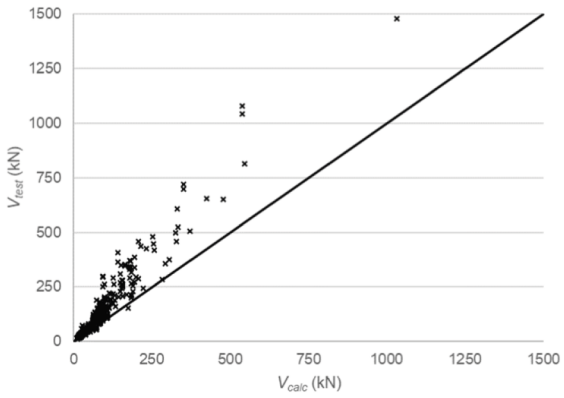

(a)

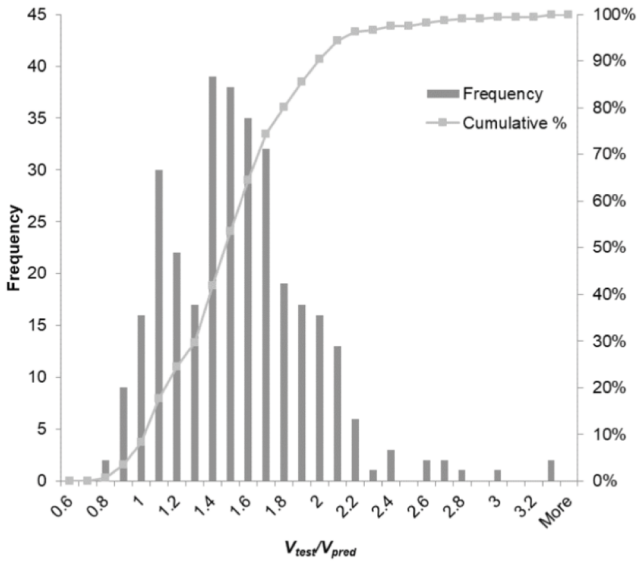

(b)

Fig. 8. Comparison between experimental shear capacity and shear capacity determined with proposed model. (a) overall comparison; (b) histogram of results.

5.2. Influence of parameters

To study the robustness of the proposed model over ranges of parameters, the ratios of tested to predicted results are plotted as a function of the varied parameters indicated in Table 2. In addition, in Table 2, the value of a_{exp} of the linear trendline between V_{test}/V_{pred} and the studied parameter (of $y = a_{exp}x + b_{exp}$ with $\times$ the studied parameter and $y = V_{test}/V_{pred}$) as well as the R^2 value are given. These values are of course

related to one single parameter at a time, and thus cannot consider the interaction between the parameters on the model, so that the resulting R^2 values are very low. However, the results give us an indication that the four parameters that have the best goodness of fit to the model are (ranked from highest R^2 to lowest): ρ, d, b and f_{tenf}. Similarly, the four parameters that have the worst goodness of fit to the model are (ranked from lowest R^2 value to highest): f_c, f_{sy}, $d_{a,\max}$ and V_f.

In total, 32 experiments have a value of $V_{test}/V_{pred} > 2$. To understand for which sets of parameters the model becomes overly conservative, these 32 experiments are studied in further detail. These experiments result from 10 Refs.: [69,71,73,79–81,86,87,91,106]. The ranges of parameters that characterize these experiments are generally in line with the ranges of the full database, except for the a/d ratio. All these experiments lie in the range between $a/d = 2.5$ to 3.5. In this range of values for the shear slenderness, shear-compression failures can govern over flexural shear failures. While the transition point between shear-compression and flexural shear failures is traditionally taken at $a/d = 2.5$, this value is in fact a function of the reinforcement ratio [107] and can be up to 4.5 in prestressed concrete [108]. Since the reinforcement ratios in this subset of 32 experiments are high (1.3–4.5 %) and we have the addition of the steel fibers, it is plausible to assume that the ultimate capacity of these members was increased as a result of arching action, which is not considered in the proposed model.

In this section, the results regarding the parameters that are of interest are further highlighted: the width b, the effect depth d, the shear slenderness a/d, the reinforcement ratio ρ, the concrete compressive strength f_c, the maximum aggregate size $d_{a,\max}$, the fiber factor F, the fiber volume fraction V_f, and the fiber tensile strength f_{tenf}.

Fig. 9 shows the influence of the width (b) and the width-to-depth ratio (b/d). From Fig. 9a we can observe a tendency for the model underestimate the effect of the width, which may be attributed to the transverse distribution capacity of wider members and the undulation of the wider shear crack, which provides more aggregate interlock capacity. Plotting the results as a function of b/d, Fig. 9b, shows a less clear influence of the width [109]. For small values of b/d the results of experiments with $a/d \geq$ and $<$ 3.5 are similar, whereas the number of experiments with $b/d > 1$ is limited. The model tends to underestimate the capacity for the experiments with $b/d > 1$ (with two exceptions), and this observation is especially true for the experiments with $a/d < 3.5$. This observation can be related to the influence of the width on the relation between shear capacity and position of the load as previously reported for slabs [110] and also confirms the findings of Conforti et al.

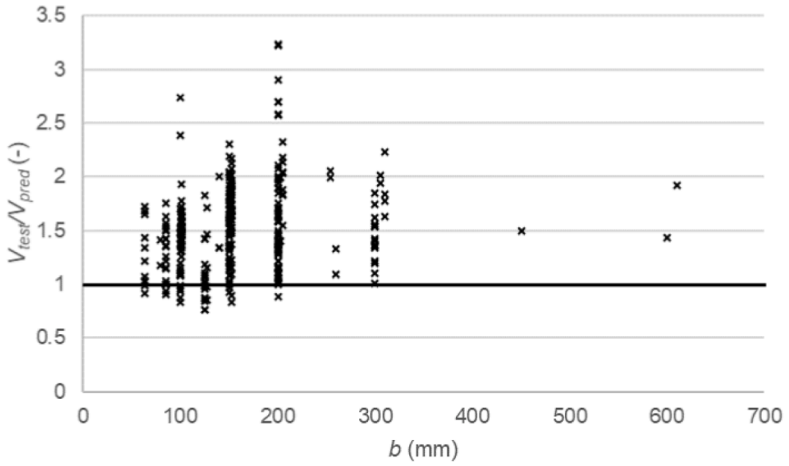

(a)

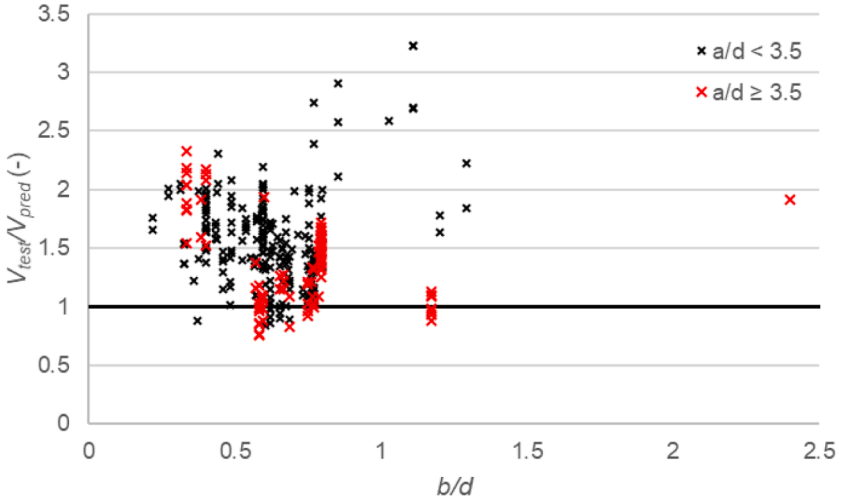

(b)

Fig. 9. Relation between tested to predicted ratio and: (a) specimen width and (b) width to depth ratio, subdivided by results with a/d $<$ 3.5 and a/d $\geq$ 3.5.

[83] that in the range of b/d between 1 and 3, the shear capacity is slightly larger than for more beam-like ($b/d < 1$) and more slab-like (often defined as $b/d > 5$) members. This observation can be explained by the way in which both the width of the member and shear slenderness influence the development of a compressive arch between the load and the support.

All in all, experiments on wide members with SFRC are scarce, and further experimental research may be necessary to identify the influence of the width. In future experiments, the use of advanced instrumentation techniques will be valuable to identify in the transverse distribution in the member, as well as identify the shear-carrying mechanisms from the crack kinematics. For the proposed model, the width can influence the assumed shape of the shear crack, and a more undulated crack over the width direction can result in a larger plane to provide shear resistance and thus a larger shear capacity. Such modifications to the model can be developed when more experimental evidence becomes available.

The second parameter to study in more detail is the effective depth d. It is known [111] that the shear capacity of reinforced concrete members without shear reinforcement does not increase proportionally as the depth of the member increases. This observation is named the size effect in shear. On the other hand, adding steel fibers to the mix has shown to reduce the size effect in shear [45]. In the proposed model, the aggregate interlock capacity is related to the size effect through the crack width, whereas the capacity provided by the steel fibers in the tension zone is not influenced by the member depth. Fig. 10 shows that the results are as well related to the position of the load (a/d) and that the members in which arching action could occur show an opposite trend than those with a larger shear slenderness.

The third parameter to study in more detail is the shear span to depth ratio. For reinforced concrete, it is known [107,112] that the moment at which shear capacity occurs over the flexural capacity has a minimum for a certain value around $a/d = 2.5$. The exact value depends on the reinforcement ratio. The effect can be expressed as the shear span to depth ratio a/d, the clear shear span to depth ratio a_v/d or as the moment to shear ratio M/Vd, which may be preferable for continuous members. As the specimens in the database are mostly simply supported beams subjected to one or two concentrated loads, the ratio a_v/d is appropriate, because it also considers the size of the loading and support plates. Fig. 11 shows that for SFRC concrete members, an increase in shear capacity occurs as the load is placed closer to the support. The exact a_v/d ratio at which the increase starts cannot be directly indicated, as it appears to be a function of the reinforcement ratio and the fibers. The ratio appears to be equal to or larger than the ratio for reinforced concrete members without transverse reinforcement, and the analysis of the underpredictions of the proposed model already indicated that members with a large reinforcement ratio and a/d between 2.5 and 3.5 can benefit from arching action.

The fourth parameter to study is the effect of the longitudinal

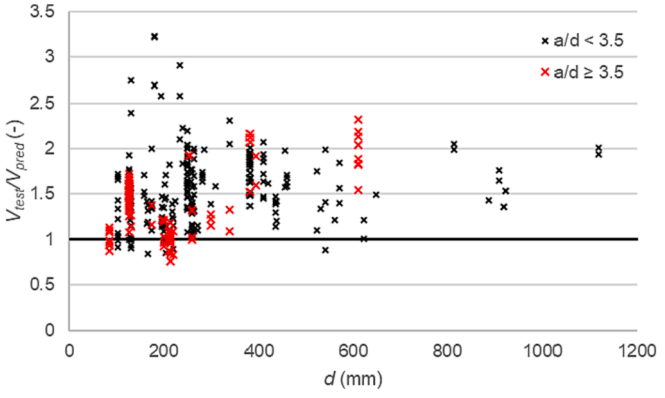

Fig. 10. Relation between tested to predicted ratio and effective depth of the specimen.

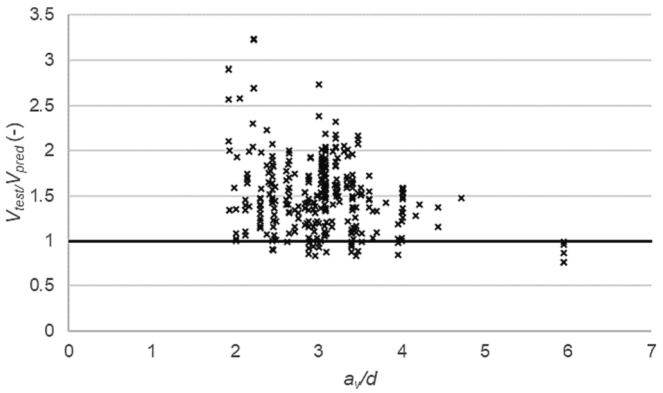

Fig. 11. Relation between clear shear span to depth ratio and tested to predicted ratio.

reinforcement. The longitudinal reinforcement provides shear capacity through dowel action, see Eq. (5). The longitudinal reinforcement ratio also has a large influence on the internal equilibrium of forces, and thus influences the height of the compression zone, and thus the contribution of the uncracked compression zone. As can be seen in Fig. 12a, the ratio of tested to predicted capacities is uniform over the range of reinforcement ratios that are tested. It should be noted that the vast majority of experiments are heavily reinforced, with $\rho \geq 1$ %, so that experiments with lower reinforcement ratios are necessary. The effect of ρ is taken into account in the model through the expression of dowel action, where it is indirectly considered through the number and diameter of the reinforcement bars. Through the equilibrium of the section, the reinforcement ratio also influences the contribution of the concrete compression zone. The yield strength of the steel influences the ratio of tested to predicted capacities, see Fig. 12b. For higher steel strengths, it appears that arching action plays a more prominent role. In addition, improvements to the model could look into considering the yield strength of the steel into the dowel action expression.

The fifth property to study is the influence of the concrete in terms of the concrete compressive strength and the maximum aggregate size. The concrete compressive strength is often considered as one of the main parameters to the shear capacity of concrete members, and it influences all shear-carrying mechanisms. As can be seen in Fig. 13a, this model performs well over a wide range of concrete compressive strengths, especially for experiments with $a/d \geq 3.5$. Additionally, the maximum aggregate size influences the aggregate interlock capacity. In the considered experiments, some concrete mixes use particularly small values for the maximum aggregate size. As can be seen in Fig. 13b, the model performs uniformly over a wide range of values of the maximum aggregate size. The maximum aggregate size is used in this model to estimate the cover c_a in Eq. (12). Improvements to the aggregate interlock expression could also take into account the roughness of the crack as a function of the maximum aggregate size.

The final parameter to evaluate relates to the properties and amount of fibers in the concrete mix. As theoretically identified previously [4], the presence of steel fibers influences all shear-carrying mechanisms. In the proposed model, the influence of the fibers is considered (1) on the sectional equilibrium, and thus on the height of the compression zone which determines the contribution of the concrete under compression, (2) on the aggregate interlock capacity by considering the effect of fibers on crack width and spacing, and (3) by adding the contribution of the fibers in the tension zone of the cross-section. Fig. 14a shows that the model performs uniformly over the range of fiber volume fractions that are tested. Fig. 14b shows the results as a function of the fiber factor, which indicates a larger contribution of arching action in ranges of small values of the fiber factor. This observation is in line with the knowledge that as more fibers are present in the mix, the fibers start to act like shear reinforcement, and the shear-carrying load path changes from the

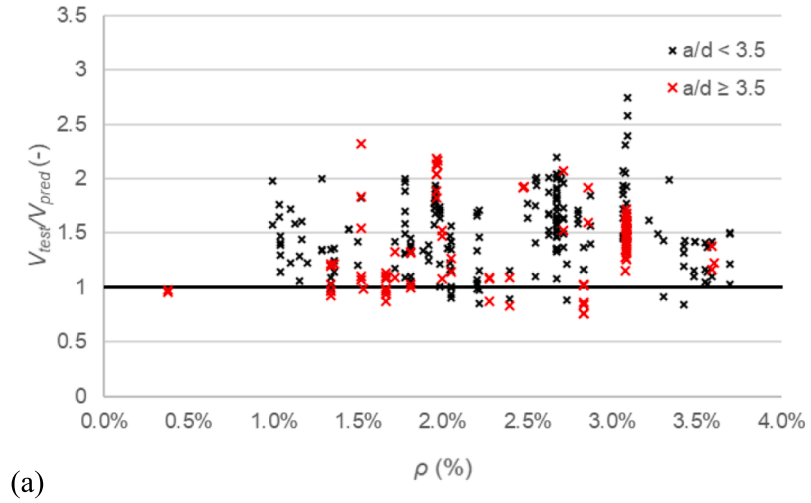

(a)

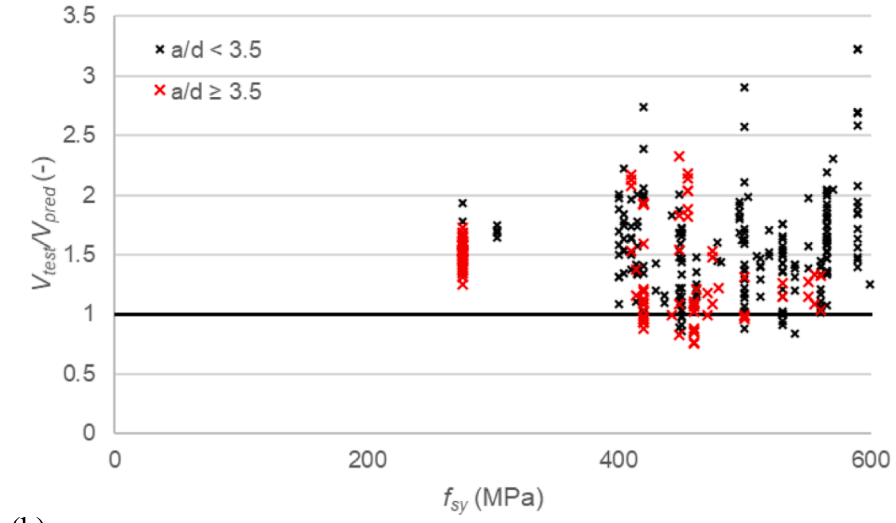

(b)

Fig. 12. Relation between longitudinal reinforcement and tested to predicted ratio: (a) reinforcement ratio, (b) yield strength of the reinforcement.

combination of the shear-carrying mechanism as considered in this model for flexure-shear failures to the truss model that is used for shear-reinforced members. This observation is also in line with the proposed approaches for the shear capacity of SFRC beams with stirrups [75,113]. In addition, Fig. 14c shows that the ratio of tested to predicted capacity is also a function of the tensile strength of the fibers, and that this factor should be considered for the fibers with a low tensile strength.

5.3. Contribution of the shear-carrying mechanisms

For the 310 out of 323 experiments for which the model indicates a shear failure and not a flexural failure, the contribution of the shear-carrying mechanisms can be determined. For this purpose, the values of the calculated contribution of the compression zone, fibers across the crack, aggregate interlock, and dowel action are compared to the total predicted capacity. The resulting values as percentages indicate the theoretical contribution of each of these mechanisms. Table 3 shows the results for the four studied shear-carrying mechanisms. From these results, we can observe that on average the contribution of the concrete in the compression zone is the largest, and that the contribution of dowel action is the smallest. Wide ranges of contributions are found for the fibers in the tension zone and for aggregate interlock, which is in line with the assumptions in the model.

Then, we can study the influence of different parameters on the contributions of the various shear-carrying mechanisms. Fig. 15a shows that dowel action remains relatively constant as a function of the reinforcement ratio. While a larger amount of reinforcement leads to a larger absolute value of the dowel action, the internal equilibrium leads as well to a larger contribution of the compression zone, so that the relative contribution of the dowel action remains similar. On the other hand, Fig. 15b shows that the contribution of dowel action reduces as the fiber factor increases. As the fiber factor increases, the influence of the fibers becomes more important, and the contribution of the other shear-carrying mechanisms reduces.

Fig. 16a shows that the contribution of the concrete compression zone increases as the concrete compressive strength increases, as expected. The increase is however moderate. Fig. 16b shows that the contribution of the concrete compression zone increases as the reinforcement ratio increases, as a result of the larger height of the compression zone necessary for the equilibrium.

Fig. 17 shows that, as expected, the contribution of the fibers in the tension zone increases as the fiber factor increases. Fig. 18 shows the opposite effect for aggregate interlock: the contribution of aggregate interlock reduces as the fiber factor increases. As such, we can see that

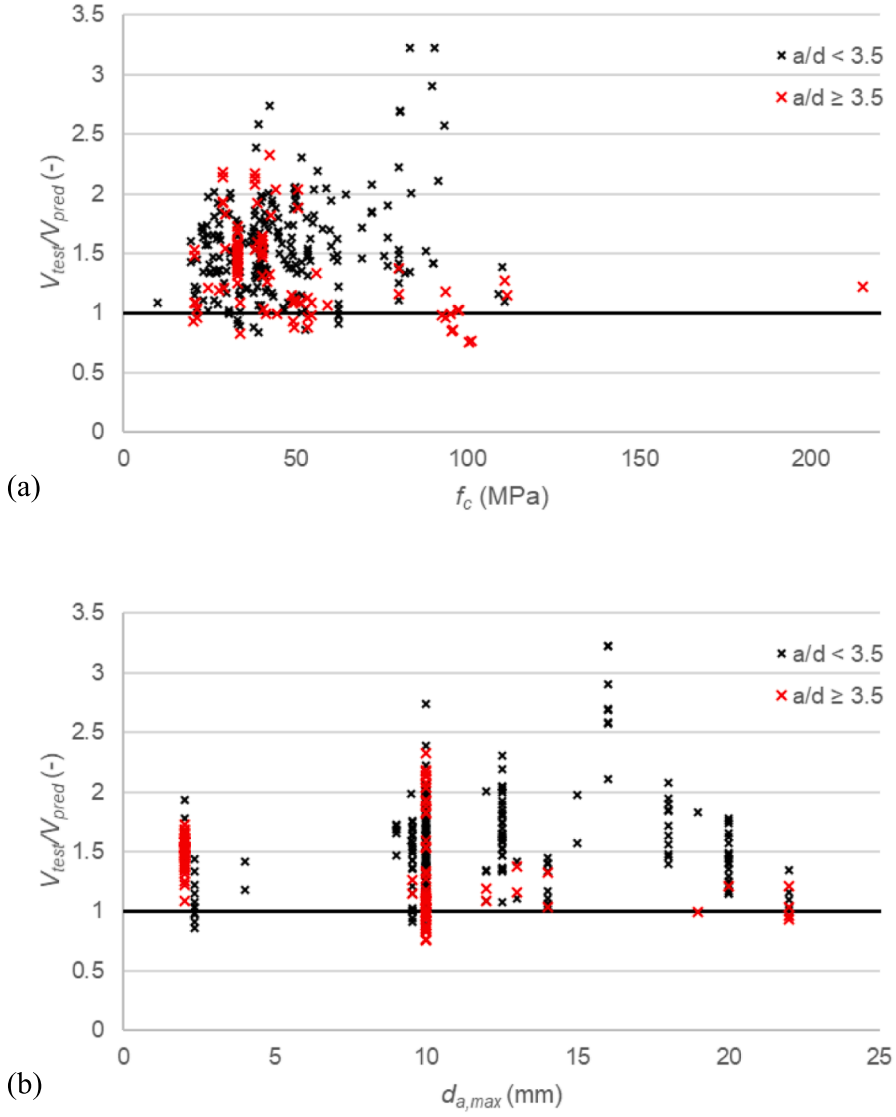

Fig. 13. Relation between properties of the concrete mix and tested to predicted ratio: (a) concrete compressive strength; (b) maximum aggregate size.

the mechanism to transfer shear in the tension zone changes from mostly aggregate interlock to mostly the transfer by the fibers. As such, this result also shows that the assumption used in various models to add the contribution of the fibers to the contribution of the concrete is not correct, as there is an interaction between the shear-carrying mechanisms in the tension zone.

6. Discussion

6.1. Value of theoretical model based on shear-carrying mechanisms

The strength of the currently proposed model lies in the fact that it is entirely based on theoretical considerations and existing descriptions of the shear-carrying mechanisms. No additional sources of empiricism have been added to this model. As such, it provides a framework for further theoretical developments and for the design of targeted experimental campaigns to better understand the shear-carrying mechanisms and shear capacity of SFRC members.

While other models as reported in the literature and compared to different datasets may have a better performance in terms of the coefficient of variation [68], this model can be considered as a theoretical framework that can be further developed and refined, as more experimental insights become available.

6.2. Path towards improvement of model

Experimental evidence is necessary to further develop the model. Experiments should be carried out in which digital image correlation (DIC) is used to study the crack kinematics [114], to study the critical shear displacement [22], and to track the slipping and sliding of the cracks, so that the aggregate interlock model can be refined for SFRC. In addition, advances in the use of acoustic emission measurements [115] can be used to map the development of internal cracking, and fiber optic sensors can be slotted into the reinforcement to compare the strains from the sectional model with the strains in the reinforcement in the experiment [116,117]. With this information, the simplification of using the flexural cracking model for SFRC can be circumvented and the critical shear displacement of a SFRC member failing in shear can be studied. Moreover, the application of the sectional model can be validated, and the development of the crack internally can be captured better.

The experimental insights can then be used to study various open questions. The first open question is the cross-section where the analysis

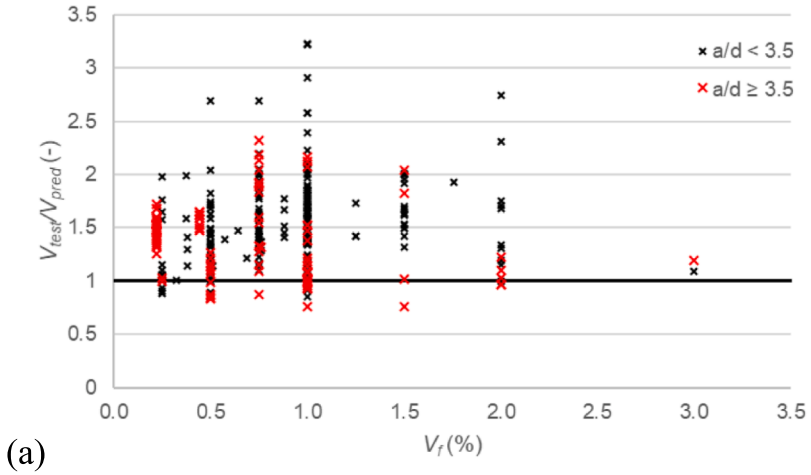

(a)

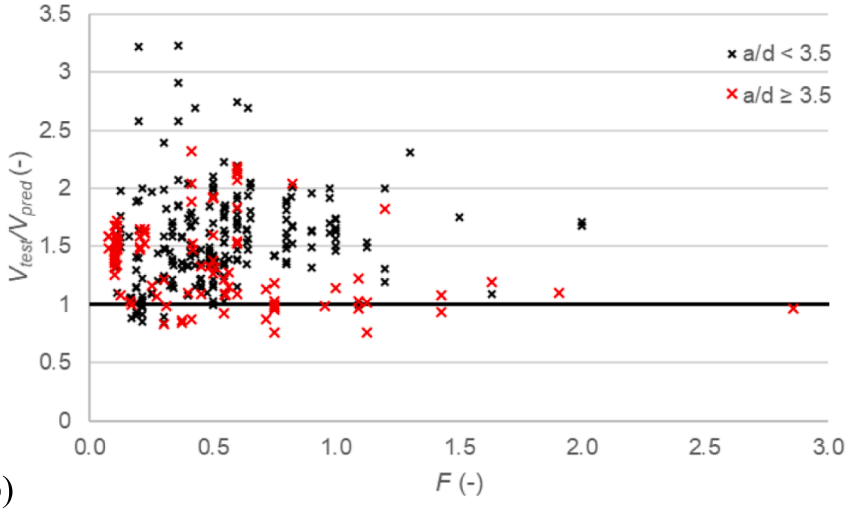

(b)

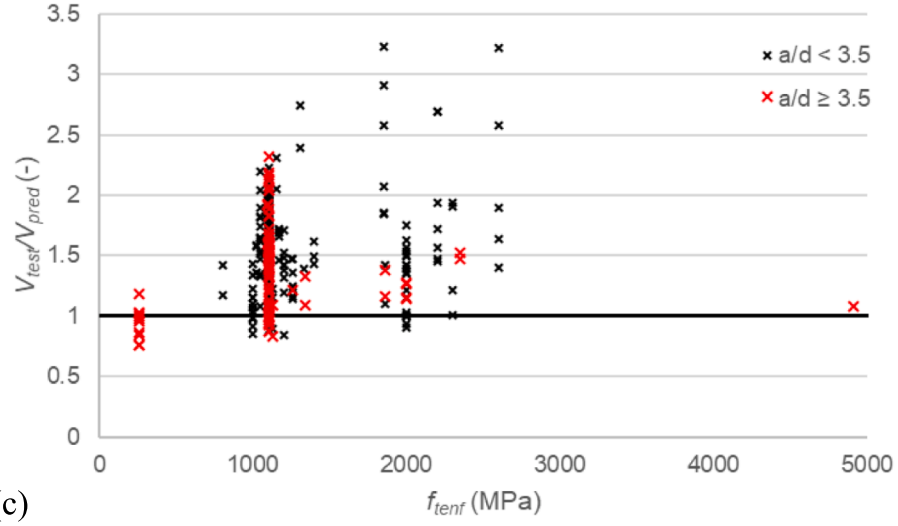

(c)

Fig. 14. Relation between fiber properties and tested to predicted ratio: (a) fiber volume fraction; (b) fiber factor; (c) fiber tensile strength.

Table 3
Theoretically derived ranges of contribution of the shear-carrying mechanisms.

Mechanism	Avg	Min	Max
Dowel action	15 %	2 %	33 %
Concrete in compression zone	41 %	18 %	52 %
Fibers in tension zone	22 %	4 %	55 %
Aggregate interlock	22 %	5%	47 %

should be carried out. At this moment, the analysis is carried out at the cross-section which has the largest shear demand. However, other models [118] propose different positions. Positions that are considered in other solutions include: at a distance d from the support or from the load, or at the location where the shear crack crosses the mid-height of the cross-section. The latter may perhaps be the most appropriate approach for a model that is based on the shear-carrying mechanisms, but requires a better understanding of the inclination of the shear crack. The inclination, position, and shape of the shear crack are currently not logged in the experimental database [68]. Moreover, new experimental results are necessary to properly document the position, inclination, and shape of the shear crack, and crack development, as well as to use DIC analysis to find the angle of the principal strains. The information of the shear crack could then be used to go from a one-dimensional sectional analysis to taking the positions of the contributions according to Fig. 1 into account.

The second open question relates to the dowel action capacity in SFRC members. At this moment, the same expression is used as for reinforced concrete members. Another model that was used for comparison, but not included in the proposed model, is the dowel action model for SFRC [119]. This dowel action model for SFRC, however, results in much higher contributions of dowel action, which seem to overestimate the contribution of this mechanism. As such, further research on dowel action in SFRC is necessary. This observation ties in with the conclusion from the parameter studies, which stated that the yield strength of the steel reinforcement should be considered in the dowel action expression as well, so that the model can be extended to members with high-strength steel reinforcement.

The third open question relates to the aggregate interlock formulation. The current limitations of the crack width to a minimum of 0.04 mm needs to be reevaluated for SFRC, in which the fibers keep the cracks closed. Moreover, the limit of $f_c = 60$ MPa should be extended as many

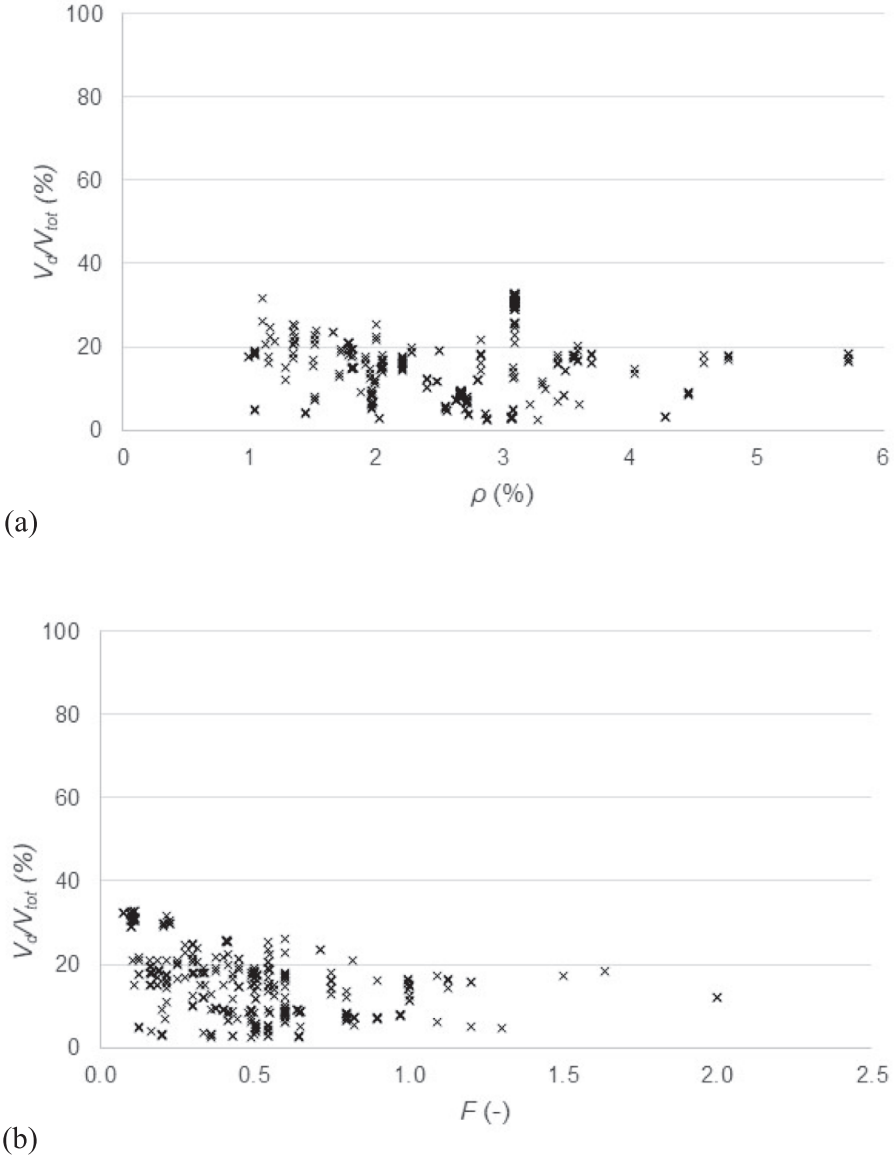

Fig. 15. Influence of parameters on the contribution of dowel action to the total predicted shear capacity: (a) reinforcement ratio; (b) fiber factor.

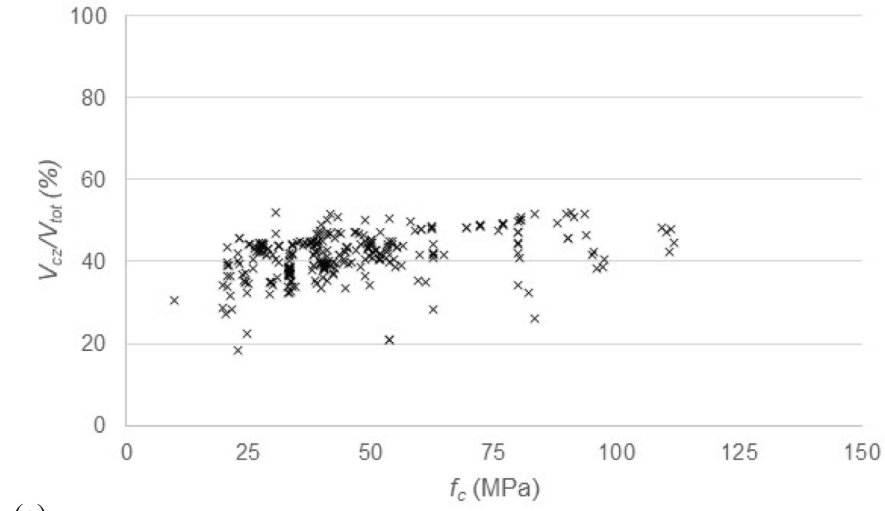

(a)

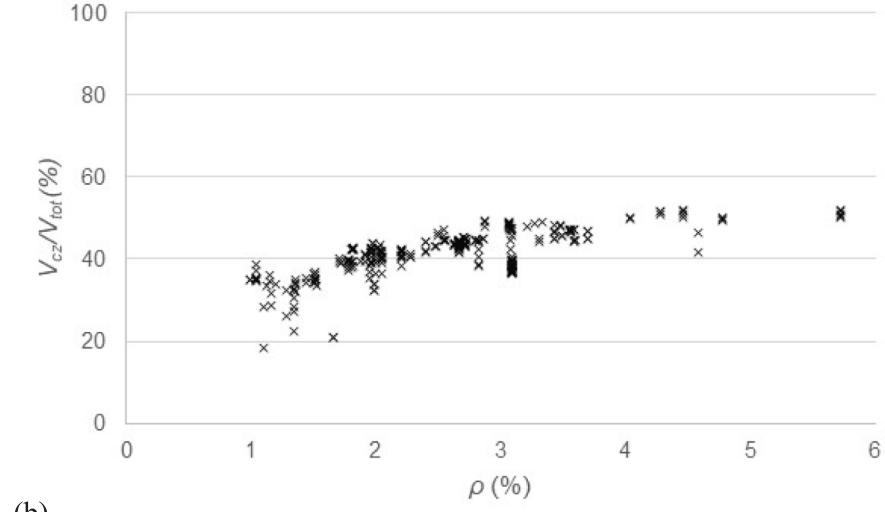

(b)

Fig. 16. Influence of parameters on the contribution of the concrete compression zone to the total predicted shear capacity: (a) concrete compressive strength; (b) reinforcement ratio.

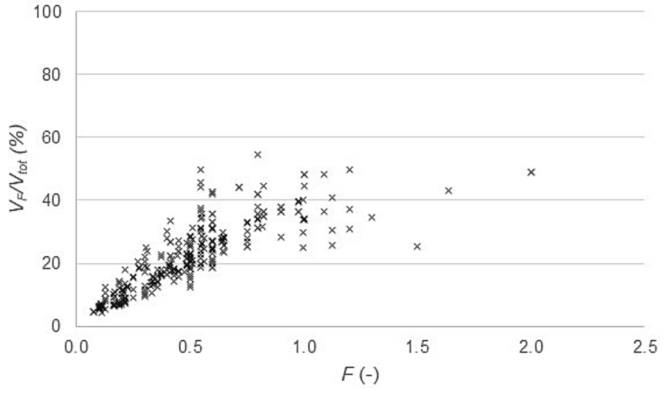

Fig. 17. Influence of fiber factor on contribution of fibers in the tension zone to the total predicted shear capacity.

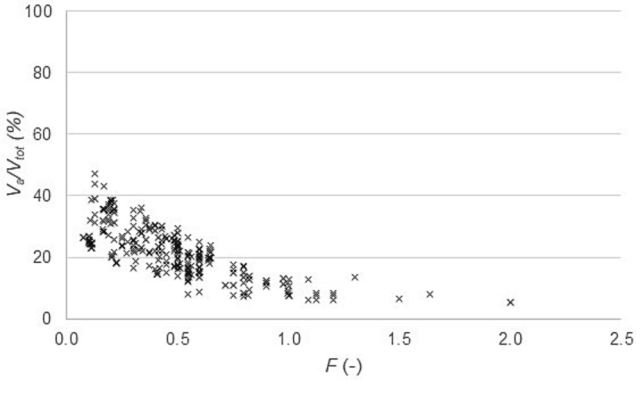

Fig. 18. Influence of fiber factor on contribution of aggregate interlock to the total predicted shear capacity.

SFRC mixes result in higher concrete compressive strengths. In addition, the use of the crack width model for flexural cracking in SFRC members is a simplification for the case of shear-critical elements and requires better quantification.

The fourth open question relates to the contribution of steel fibers in the tension zone. The expression currently does not consider the yield

strength of the fibers. While most current SFRC mixes include standard fibers, older experiments with non-standard fibers of mild steel have different bond and tension properties. Similarly, as new bio-based fiber materials and mixes are developed, it is necessary to develop expressions that explicitly take the fiber bond and tensile strength into account.

The final open question relates to the change in behavior from non-shear-reinforced behavior, consisting of the shear-carrying mechanisms, as used in this model, to the shear-reinforced behavior consisting of a truss-like mechanism. Further research should study for which fiber volume fraction or which fiber factor this transition takes place. In addition, the range of values of a/d in which shear-compression failures can occur needs to be studied further.

7. Summary and conclusions

This paper proposes a theoretical model to determine the shear capacity of SFRC members. The model is based on the shear-carrying mechanisms as used in the Critical Shear Displacement Theory and sectional analysis. The influence of the steel fibers is considered in: the sectional equilibrium, the concrete contribution through the height of the compression zone, the aggregate interlock capacity through the crack width and spacing, and the contribution of the fibers.

The proposed model is then compared to 323 experiments on rectangular, slender SFRC beams that reportedly failed in shear. This comparison shows that the model is slightly conservative with an average ratio of tested to predicted capacity of 1.50 and coefficient of variation of 26.6 %. The comparison indicates that arching action can occur up to $a/d = 3.5$ in SFRC.

After the comparison between the experimental results and the theory, a way forward to improve the model is sketched. Targeted experiments with extensive instrumentation and DIC analysis are recommended to properly address the crack kinematics of SFRC members failing in shear, as well as to address the open questions regarding the shear behavior of SFRC that are raised in this work. We can conclude that the proposed theory is a framework based on established models of the sectional equilibrium and the shear-carrying mechanisms. No empirical elements are added, and this theory lays the groundwork for a solid mechanical model for the shear capacity of SFRC.

Declaration of Competing Interest

The author declares that she has no known competing financial interests or personal relationships that could have appeared to influence the work reported in this paper.

Data availability

Data will be made available on request.

Acknowledgement

The author is grateful for the financial support provided by the program of Poligrants (2017-2018, 2018-2019) of Universidad San Francisco de Quito.

References

[1] Katzer J. Steel fibers and steel fiber reinforced concrete in civil engineering. Pac J Sci Technol 2006;7:53–8.
[2] Mark P, Heek P. Bemessung von Stahlfaserbetonbauteilen. Ruhr Universitat Bochum; 2013.
[3] ACI Committee 318. Building code requirements for structural concrete (ACI 318-19) and commentary. Farmington Hills, MI: American Concrete Institute; 2019.
[4] Lantsoght EOL. How do steel fibers improve the shear capacity of reinforced concrete beams without stirrups? . Composites Part B: Engineering. 2019;175.
[5] Vougioukas E, Papadatou M. A Model for the Prediction of the Tensile Strength of Fiber-Reinforced Concrete Members. Before and After Cracking Fibers 2017;5:27.
[6] Dinh HH. Shear behavior of steel fiber reinforced concrete beams without stirrup reinforcement. The University of Michigan; 2009.
[7] Amin A, Gilbert RI. Instantaneous Crack Width Calculation for Steel Fiber-Reinforced Concrete Flexural Members. ACI Struct J 2018;115.
[8] Imam M, Vandewalle L, Mortelmans F. Shear – moment analysis of reinforced high strength concrete beams containing steel fibres. Can J Civ Eng 1995;22:462–70.
[9] Blasón S, Poveda E, Ruiz G, Cifuentes H, Fernández CA. Twofold normalization of the cyclic creep curve of plain and steel-fiber reinforced concrete and its application to predict fatigue failure. Int J Fatigue 2019;120:215–27.
[10] Isojeh B, El-Zeghayar M, Vecchio FJ. Fatigue Resistance of Steel Fiber-Reinforced Concrete Deep Beams. ACI Struct J 2017;114.
[11] Tan KH, Paramasivam P, Tan KC. Instantaneous and Long-Term Deflections of Steel Fiber Reinforced Concrete Beams. ACI Struct J 1994;91.
[12] Sturm AB, Visintin P, Oehlers DJ, Seracino R. Time-Dependent Tension-Stiffening Mechanics of Fiber-Reinforced and Ultra-High-Performance Fiber-Reinforced Concrete. J Struct Eng 2018;144:04018122.
[13] de Sousa AMD, Lantsoght EOL, Genikomsou AS, Krahl PA, El Debs MK. Behavior and punching capacity of flat slabs with the rational use of UHPFRC: NLFEA and analytical predictions. Eng Struct 2021;244:112774.
[14] Walraven JC. Fundamental analysis of aggregate interlock. J Struct Div-ASCE 1981;107:2245–70.
[15] Vintzileou E. Shear transfer by dowel action and friction as related to size effects. CEB Bulletin 1997;237:53–77.
[16] Walraven JC. Fracture mechanics of concrete and its role in explaining structural behaviour. Fract Mech Concr Concr Struct 2007;1–3(1–3):1265–75.
[17] Zararis PD, Zararis IP. Shear Strength of Reinforced Concrete Slender Beams with or without Axial Forces-A Generalized Theory. ACI Struct J 2009;106:782–9.
[18] Mobasher B, Yao Y, Soranakom C. Analytical solutions for flexural design of hybrid steel fiber reinforced concrete beams. Eng Struct 2015;100:164–77.
[19] Soranakom C, Mobasher B. Closed-Form Solutions for Flexural Response of Fiber-Reinforced Concrete Beams. J Eng Mech 2007;133:933–41.
[20] Jordon R. Deluce S-CL, Frank JV. Crack Model for Steel Fiber-Reinforced Concrete Members Containing Conventional Reinforcement. ACI Structural Journal.111.
[21] Yang Y, Walraven J, den Uijl JA. Shear Behavior of Reinforced Concrete Beams without Transverse Reinforcement Based on Critical Shear Displacement. Journal of Structural Engineering. 2017;143:04016146-1-13.
[22] Yang Y, Den Uijl JA, Walraven J. The Critical Shear Displacement theory: on the way to extending the scope of shear design and assessment for members without shear reinforcement. Struct Concr 2016;17:790–8.
[23] Association Française de Génie Civil. Bétons fibrés à ultra-hautes performances: Recommandations. 2013. p. 359.
[24] DAfStB. DAfStB-Richtlinie Stahlfaserbeton. 2012. p. 47.
[25] fib. Model code 2010: final draft. Lausanne: International Federation for Structural Concrete; 2012.
[26] Vecchio FJ, Collins MP. The Modified Compression-Field Theory for Reinforced-Concrete Elements Subjected to Shear. J Am Concr Inst 1986;83:219–31.
[27] Muttoni A, Ruiz MF. Levels-of-Approximation Approach in Codes of Practice. Struct Eng Int 2012;22:190–4.
[28] RILEM TC 162-TDF. σ-ε-Design Method. Mater Struct. 2003;36:560-7.
[29] Lee DH, Kim KS, Han SJ, Zhang D, Kim J. Dual potential capacity model for reinforced concrete short and deep beams subjected to shear. Struct Concr 2018;19:76–85.
[30] Lee DH, Han S-J, Kim KS, LaFave JM. Shear capacity of steel fiber-reinforced concrete beams. Struct Concr 2017;18:278–91.
[31] Marì Bernat A, Spinella N, Recupero A, Cladera A. Mechanical model for the shear strength of steel fiber reinforced concrete (SFRC) beams without stirrups. Mater Struct/Materiaux et Constructions 2020;53.
[32] Kupfer H, Hilsdorf HK, Rusch H. Behavior of Concrete Under Biaxial Stresses. ACI Journal Proceedings 1969;66:656–66.
[33] Nielsen MP, Hoang LC. Limit analysis and concrete plasticity. 3rd ed. ed. Boca Raton, Fla.: CRC; 2011.
[34] Batson GB, Youssef AG. Shear Capacity of Fiber Reinforced Concrete Based on Plasticity of Concrete: A Review. ACI Special Publication. 1994;142.
[35] Lim TY, Paramasivam P, Lee SL. Shear and moment capacity of reinforced steel-fibre-concrete beams. Mag Concr Res 1987;39:148–60.
[36] Lim TY, Paramasivam P, Lee SL. Analytical Model for Tensile Behavior of Steel-Fiber Concrete. ACI Mater J 1987;84.
[37] Braestrup MW. Yield line theory and concrete plasticity. Mag Concr Res 2008;60:549–53.
[38] Lampert P, Thürlimann B. Ultimate Strength and Design of Reinforced Concrete Beams In Torsion and Bending. Publications, International Association of Bridge and Structural Engineering Zurich: ETH; 1971. p. 107-31.
[39] Spinella N. Shear strength of full-scale steel fibre-reinforced concrete beams without stirrups. Comput Concr 2013;11:365–82.
[40] Spinella N, Colajanni P, Mendola LL. Nonlinear Analysis of Beams Reinforced in Shear with Stirrups and Steel Fibers. ACI Struct J 2012;109.
[41] Spinella N, Colajanni P, Recupero A. Simple Plastic Model for Shear Critical SFRC Beams. J Struct Eng 2010;136:390–400.
[42] Autrup F, Joergensen HB. Shear capacity of RC members without shear reinforcement: A modified crack sliding model. Eng Struct 2021;239:112147.
[43] Zhang J-P. Diagonal cracking and shear strength of reinforced concrete beams. Mag Concr Res 1997;49:55–65.
[44] Narayanan R, Darwish IYS. Fiber Concrete Deep Beams in Shear. ACI Struct J 1988;85.

[45] Minelli F, Conforti A, Cuenca E, Plizzari G. Are steel fibres able to mitigate or eliminate size effect in shear? Mater Struct 2014;47:459–73.
[46] Zhang F, Ding Y, Xu J, Zhang Y, Zhu W, Shi Y. Shear strength prediction for steel fiber reinforced concrete beams without stirrups. Eng Struct 2016;127:101–16.
[47] Minelli F, Vecchio FJ. Compression Field Modeling of Fiber-Reinforced Concrete Members Under Shear Loading. ACI Struct J 2006;103.
[48] Vecchio FJ. Disturbed stress field model for reinforced concrete: Formulation. J Struct Eng-ASCE 2000;126:1070–7.
[49] Lee S-C, Cho J-Y, Vecchio FJ. Analysis of Steel Fiber-Reinforced Concrete Elements Subjected to Shear. ACI Struct J 2016;113.
[50] Wong PS, Vecchio FJ, Trommels H. VecTor 2 & FormWorks User's Manual. 2013. p. 347.
[51] Susetyo J, Gauvreau P, Vecchio FJ. Steel Fiber-Reinforced Concrete Panels in Shear: Analysis and Modeling. ACI Struct J 2013:110.
[52] Kim KS, Lee DH, Hwang J-H, Kuchma DA. Shear behavior model for steel fiber-reinforced concrete members without transverse reinforcements. Compos B Eng 2012;43:2324–34.
[53] Stevens DJ, Liu D. Constitutive Modeling of Fiber Reinforced Concrete. ACI Special. Publication 1994:142.
[54] Barros JAO, Foster SJ. An integrated approach for predicting the shear capacity of fibre reinforced concrete beams. Eng Struct 2018;174:346–57.
[55] Foster SJ, Agarwal A, Amin A. Design of steel fiber reinforced concrete beams for shear using inverse analysis for determination of residual tensile strength. Struct Concr 2018;19:129–40.
[56] Matthys S, Soetens T. Engineering Model for SFRC Shear Strength Based on MC2010 MCFT Approach. fib symposium 2017. Maastricht, the Netherlands2017.
[57] Hwang J-H, Lee DH, Kim KS, Ju H, Seo S-Y. Evaluation of shear performance of steel fibre reinforced concrete beams using a modified smeared-truss model. Mag Concr Res 2013;65:283–96.
[58] Hsu TTC. Softened Truss Model Theory for Shear and Torsion. ACI Struct J 1988;85.
[59] Hsu TTC, Mo YL. Softening of Concrete in Torsional Members - Theroy and Tests. J Proc 1985:82.
[60] Mörsch E. Der Eisenbetonbau: Seine Theorie und Anwendung. Stuttgart: Verlag Von Konrad Wiitwer; 1908.
[61] Baumann T, Rusch H. Versuche zum Studium der Verdübelungswirkung der Biegezugbewehrung eines Stahlbetonbalkens. DAfStB 1970.
[62] Yang Y. Shear Behaviour of Reinforced Concrete Members without Shear Reinforcement - A New Look at an Old Problem. Delft: Delft University of Technology; 2014.
[63] Walraven J. Aggregate interlock: a theoretical and experimental analysis. Delft, The Netherlands: Delft University of Technology; 1980.
[64] Mansur MA, Ong KCG, Paramasivam P. Shear Strength of Fibrous Concrete Beams Without Stirrups. J Struct Eng 1986;112:2066–79.
[65] Park MK, Lantsoght EOL, Zarate Garnica GI, Yang Y, Sliedrecht H. Analysis of Shear Capacity of Prestressed Concrete Bridge Girders. ACI Struct J 2021;118.
[66] Roosen MA, Van der Veen C, Hordijk DA, Hendriks MAN. Shear tension resistance of prestressed girders with a low stirrup ratio. SEMC 2019. Cape Town, South Africa2019.
[67] Bae BI, Choi HK, Choi CS. Flexural and Shear Capacity Evaluation of Reinforced Ultra-High Strength Concrete Members with Steel Rebars. Key Eng Mater 2014;577–578:17–20.
[68] Lantsoght EOL. Database of Shear Experiments on Steel Fiber Reinforced Concrete Beams without Stirrups Materials. 2019;12:917.
[69] Singh B, Jain K. An appraisal of steel fibers as minimum shear reinforcement in concrete beams (with Appendix). ACI Struct J 2014;111.
[70] Sahoo DR, Sharma A. Effect of Steel Fiber Content on Behavior of Concrete Beams with and without Stirrups. ACI Struct J 2014;111:1157–66.
[71] Manju R, S. S, B. S. Shear strength of high-strength steel fibre reinforced concrete rectangular beams. International Journal of Civil Engineering and Technology 2017;8:1716-29.
[72] Arslan G, Keskin RSO, Ulusoy S. An experimental study on the shear strength of SFRC beams without stirrups. J Theor Appl Mech 2017;55.
[73] Parra-Montesinos GJ, Wight JK, Dinh HH, Libbrecht A, Padilla C. Shear strength of fiber reinforced concrete beams without stirrups. Report No UMCEE 06-04. Ann Arbor, MI: University of Michigan; 2006. p. 39.
[74] Rosenbusch J, Teutsch M. Trial beams in shear Brite/Euram Project 97–4163 Final Rep. Sub Task 4.2. Braunschweig, Germany: Technical University of Braunschweig; 2003. p. 105–17.
[75] Amin A, Foster SJ. Shear strength of steel fibre reinforced concrete beams with stirrups. Eng Struct 2016;111:323–32.
[76] Narayanan R, Darwish IYS. Use of Steel Fibers as Shear Reinforcement. ACI Struct J 1987;84.
[77] Cucchiara C, La Mendola L, Papia M. Effectiveness of stirrups and steel fibres as shear reinforcement. Cem Concr Compos 2004;26:777–86.
[78] Kwak Y-K, Eberhard MO, Kim W-S, Kim J. Shear Strength of Steel Fiber-Reinforced Concrete Beams without Stirrups. ACI Struct J 2002;99.
[79] Lim DH, Oh BH. Experimental and theoretical investigation on the shear of steel fibre reinforced concrete beams. Eng Struct 1999;21:937–44.
[80] Dinh HH, Parra-Montesinos GJ, Wight JK. Shear Behavior of Steel Fiber-Reinforced Concrete Beams without Stirrup Reinforcement. ACI Struct J 2010;107.
[81] Lima Araujo D, Tibúrcio Nunes FG, Toledo Filho RD, Souza de Andrade MA. Shear strength of steel fiber-reinforced concrete beams. Acta Scientiarum 2014;36:389–97.
[82] Aoude H, Belghiti M, Cook WD, Mitchell D. Response of Steel Fiber-Reinforced Concrete Beams with and without Stirrups. ACI Struct J 2012;109.
[83] Conforti A, Minelli F, Plizzari GA. Wide-shallow beams with and without steel fibres: A peculiar behaviour in shear and flexure. Compos B 2013;51:282–90.
[84] Kang T-H-K, Kim W, Kwak Y-K, Hong S-G. Shear Testing of Steel Fiber-Reinforced Lightweight Concrete Beams without Web Reinforcement. ACI Struct J 2011;108.
[85] Casanova P, Rossi P. High-Strength Concrete Beams Submitted to Shear: Steel Fibers Versus Stirrups. ACI Special Publication: Structural Applications of Fiber Reinforced Concrete 1999;182.
[86] Zarrinpour MR, Chao S-H. Shear Strength Enhancement Mechanisms of Steel Fiber- Reinforced Concrete Slender Beams. ACI Struct J 2017;114.
[87] Noghabai K. Beams of Fibrous Concrete in Shear and Bending: Experiment and Model. J Struct Eng 2000;126:243–51.
[88] Ashour SA, Hasanain GS, Wafa FF. Shear Behavior of High-Strength Fiber Reinforced Concrete Beams. ACI Struct J 1992;89.
[89] Kim C-G, Lee H, Park H-G, Hong G-H, Kang S-M. Effect of Steel Fibers on Minimum Shear Reinforcement of High-Strength Concrete Beams. ACI Struct J 2017;114.
[90] Li VC, Ward R, Hamza AM. Steel and Synthetic Fibers as Shear Reinforcement. ACI Mater J 1992;89.
[91] Greenough T, Nehdi M. Shear Behavior of Fiber-Reinforced Self-Consolidating Concrete Slender Beams. ACI Mater J 2008;105.
[92] Kang THK, Kim W, Massone LM, Galleguillos TA. Shear-Flexure Coupling Behavior of Steel Fiber-Reinforced Concrete Beams. ACI Struct J 2012;109:435–44.
[93] Dupont D, Vandewalle L. Shear Capacity of Concrete Beams Containing Longitudinal Reinforcement and Steel Fibers. ACI Special Publication. 2003;216.
[94] Batson G, Jenkins E, Spatney R. Steel Fibers as Shear Reinforcement in Beams. ACI J. Proc. 1972:69.
[95] Jindal RL. Shear and Moment Capacities of Steel Fiber Reinforced Concrete Beams. ACI Special Publication. 1984;SP 81.
[96] Shin S-W, Oh J-G, Ghosh SK. Shear Behavior of Laboratory-Sized High-Strength Concrete Beams Reinforced With Bars and Steel Fibers. ACI Special Publication. 1994;142.
[97] Imam M, Vandewalle L, Mortelmans F. Shear Capacity of Steel Fiber High-Strength Concrete Beams. ACI Special Publication High Performance Concrete. 1994;149.
[98] Kwak K-H, Suh J, Hsu C-T-T. Shear-Fatigue Behavior of Steel Fiber Reinforced Concrete Beams. ACI Struct J 1991:88.
[99] Cohen M, Aoude H. Shear behavior of SFRC and SCFRC beams. 3rd International Structural Specialty Conference. Edmonton, Alberta2012.
[100] Aoude H, Cohen M. Shear response of SFRC beams constructed with SCC and Steel Fibers. Electron J Struct Eng 2014;14:71–83.
[101] Furlan S, de Hanai JB. Shear behaviour of fiber reinforced concrete beams. Cem Concr Compos 1997;19:359–66.
[102] Dancygier AN, Savir Z. Effects of Steel Fibers on Shear Behavior of High-Strength Reinforced Concrete Beams. Adv Struct Eng 2011;14:745–61.
[103] Krassowska J, Kosior-Kazberuk M. Failure mode in shear of steel fiber reinforced concrete beams. MATEC Web Conf 2018;163:02003.
[104] Yoo D-Y, Yang J-M. Effects of stirrup, steel fiber, and beam size on shear behavior of high-strength concrete beams. Cem Concr Compos 2018;87:137–48.
[105] Shoaib A, Lubell AS, Bindiganavile VS. Size Effect in Shear for Steel Fiber-Reinforced Concrete Members without Stirrups. ACI Struct J 2014;111:1081–9.
[106] Shoaib A. Shear in Steel Fiber Reinforced Concrete without Stirrups. Edmonton, AB, CA: University of Alberta; 2012.
[107] Kani GNJ. Basic Facts Concerning Shear Failure. ACI Journal Proceedings 1966;63:675–92.
[108] Lantsoght EOL, Zarate G, Zhang F, Yang Y, Park M, Sliedrecht H. Shear experiments of prestressed concrete bridge girders. ACI Struct J 2021;118:117–30.
[109] de Sousa AMD, Lantsoght EOL, El Debs MK. One-way shear strength of wide reinforced concrete members without stirrups. Struct Concr 2021;22:968–92.
[110] Lantsoght EOL, van der Veen C, Walraven JC. Shear in One-way Slabs under a Concentrated Load close to the support. ACI Struct J 2013;110:275–84.
[111] Bazant ZP, Kazemi MT. Size effect on Diagonal Shear Failure of Beams without Stirrups. ACI Struct J 1991;88:268–76.
[112] Kani GNJ. The Riddle of Shear Failure and Its Solution. ACI J Proc 1964;61:441–67.
[113] Colajanni P, La Mendola L, Mancini G, Recupero A, Spinella N. Shear capacity in concrete beams reinforced by stirrups with two different inclinations. Eng Struct 2014;81:444–53.
[114] Campana S, Anastasi A, Ruiz MF, Muttoni A. Analysis of shear-transfer actions on one-way RC members based on measured cracking pattern and failure kinematics. Mag Concr Res 2013;65:386–404.
[115] Zhang F. Acoustic emission-based indicators of shear failure of reinforced concrete structures without shear reinforcement. Delft University of Technology; 2022.
[116] Ungermann J, Schmidt P, Classen M, Hegger J. Eccentric punching tests on column bases – New insights into the inner concrete strain development. Eng Struct 2022;262:114273.
[117] Casas JR, Barrias A. Monitoring of shear cracking in partially prestressed concrete beams by distributed optical fiber sensors. IABMAS 20162016.
[118] Muttoni A, Fernández M. Consistent design against punching shear with the Critical Shear Crack Theory: mechanical model and code implementation. 2015.
[119] Resende TLd, C T Cardoso D, C D Shehata L. Influence of steel fibers on the dowel action of RC beams without stirrups. Engineering Structures. 2020;221:111044.